Int. J. Electrochem. Sci., 15 **(2020)** 6188 – 6197, doi: 10.20964/2020.07.77

International Journal of
ELECTROCHEMICAL
SCIENCE
www.electrochemsci.org

A Facile and Eco-Friendly Approach to Synthesis of Spinel $LiMn_2O_4$ with High Electrochemical Performance

Wei Zhang[1], *Zidong Zhao*[2*], *Yun Lei*[3], *Jing Xing*[1], *Xueman Cao*[1]

[1] School of Energy and Water Resources, Shenyang Institute of Technology, Fushun 113122, China
[2] Department of Mining Engineering and Metallurgical Engineering, Western Australian School of Mines, Curtin University, Kalgoorlie 6430, Australia
[3] Shenyang Research Institute, China Coal Technology & Engineering Group Corp, Fushun 113122, China
[*]E-mail: zidongzhao@163.com

Received: 18 March 2020 / *Accepted:* 8 May 2020 / *Published:* 10 June 2020

$LiMn_2O_4$ cathode material have been prepared by sodium carbonate co-precipitation route and high temperature solid phase methods. The structural, morphological and electrochemical performance of $LiMn_2O_4$ were studied by X-ray diffraction, scanning electron microscope, galvanostatic testing, cyclic voltammetry and electrochemical impedance. The experimental results exhibited that $LiMn_2O_4$ prepared by sodium carbonate co-precipitation had a better performance. Its initial discharge capacities were 114.5, 82.1, 72.3 and 56.4 $mAh \cdot g^{-1}$ at the rates of 0.2, 2.0, 5.0 and 10 C, respectively. After 200 cycles, discharge capacity was 85.0 $mAh \cdot g^{-1}$ at a rate of 2.0 C with the capacity retention of 90.2%. It is concluded that sodium carbonate co-precipitation route is a promising method for synthesis of $LiMn_2O_4$.

Keywords: $LiMn_2O_4$; Cathode material; co-precipitation; Electrochemical performance

1. INTRODUCTION

Lithium-ion batteries have been extensive applied to power portable electronic devices [1,2], own to their excellent portability, high power density and outstanding service life [3,4]. Compared with other cathode materials for lithium-ion batteries, for instance, $LiCoO_2$ [5] and $LiNi_{0.5}Co_{0.2}Mn_{0.3}O_2$ [6], the spinel $LiMn_2O_4$ cathode material has received more and more attention because of its low cost, abundant of Mn resources, high voltage and good thermal stability [7,8].

However, the structural degradation cause by Jahn-Teller [9], causes of $LiMn_2O_4$, and the dissolution of Mn^{3+} in electrolyte [10], $LiMn_2O_4$ cathode has an unsatisfactory cycling life which limits its widespread application. Therefore, it is a research direction to improve the cycling stability of

$LiMn_2O_4$ cathode. According to literature, doping with elements [11,12], coating materials [13,14] and reducing crystal size [15,16] have been used to improve cycling stability and rate performance of $LiMn_2O_4$.

Morphologies and crystal size of $LiMn_2O_4$ often affected by the synthesis methods. Therefore, numerous methods have widely been used to synthesize $LiMn_2O_4$ such as solid-state reaction method [17,18], precipitation method [19], hydrothermal method [20], high temperature ball milling method [21], sol-gel method [22,23] and spray-dried method [24].

In the present work, $LiMn_2O_4$ materials were synthesized via co-precipitation route with sodium carbonate (Na_2CO_3) used as precipitant. Compared with traditional precipitation method used to prepare $LiMn_2O_4$, sodium carbonate co-precipitation route can simultaneously make Li^+ and Mn^{2+} precipitate, thereby obtaining a more uniform $Li_2CO_3 \cdot 2MnCO_3$ as precursor, and can reduce the reaction steps and improve the efficiency. The precipitate of manganese is $MnCO_3$, which has stable redox performance and is not easy to be converted into tetravalent. Sodium carbonate co-precipitation route can prevent Mn^{2+} from being oxidized to Mn^{4+}.

2. EXPERIMENTAL

2.1 Material preparation

The raw materials are manganese (II) acetate tetrahydrate ($Mn(CH_3COO)_2 \cdot 4H_2O$, AR), lithium acetate dihydrate ($CH_3COOLi \cdot 2H_2O$, AR), sodium carbonate (Na_2CO_3, AR). All chemistry reagents used are of analytical grade

2.1.1. Co-precipitation method (CP)

The amounts of $CH_3COOLi \cdot 2H_2O$, $Mn(CH_3COO)_2 \cdot 4H_2O$ and Na_2CO_3 were with a molar ratio of 1.03:2:2.6. Under water bath conditions, $CH_3COOLi \cdot 2H_2O$ (0.103 mol) and $Mn(CH_3COO)_2 \cdot 4H_2O$ (0.2 mol) were soluble in the deionized water with the temperature at 80-90 °C. At the same time, Na_2CO_3 (0.26 mol) was fed into the solution, then under stirring for 2 h, the precipitated $0.5Li_2CO_3 \cdot 2MnCO_3$ was filtered, washed, and dried at 120 °C for 12 h. The obtained precursor was pre-treated at 500 °C for 5 h, then sintering at 750 °C for 12 h to prepared $LiMn_2O_4$ (nominated as LMO-C). Schematic illustration of co-precipitation method is illustrated in Fig.1.

The reactions of synthesized LMO-C can be summarized as follows:

$$LiAc+2Mn(Ac)_2+\frac{5}{2}Na_2CO_3 \xrightarrow{80\text{-}90^{\circ}C} \frac{1}{2}Li_2CO_3\downarrow+2MnCO_3\downarrow+5NaAc \quad (1)$$

$$\frac{1}{2}Li_2CO_3+2MnCO_3+\frac{3}{4}O_2 \xrightarrow{750^{\circ}C} LiMn_2O_4+\frac{5}{2}CO_2 \quad (2)$$

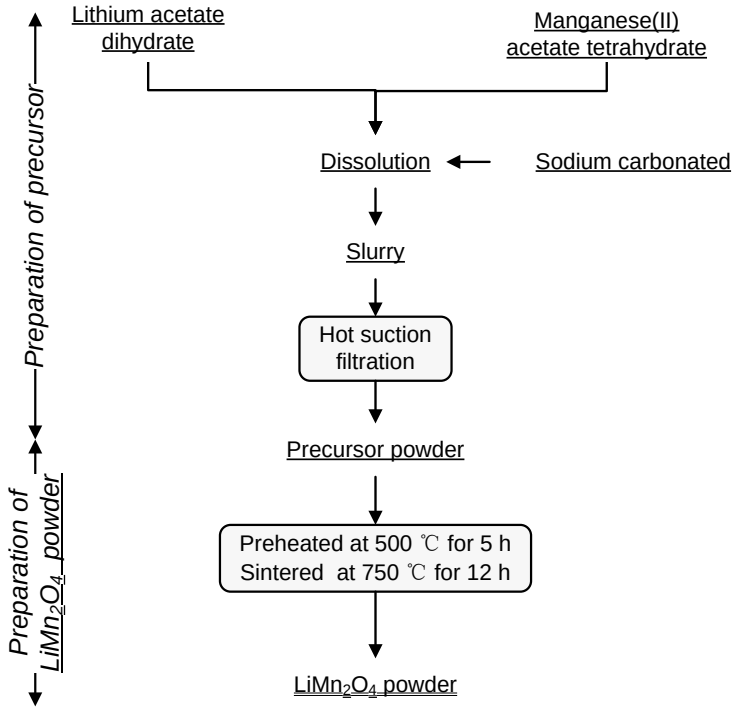

Figure 1. Schematic illustration of synthesis processes of LMO-C.

2.1.2. High temperature solid phase method (SP)

Under water bath conditions, $CH_3COOLi \cdot 2H_2O$ (0.103 mol) and $Mn(CH_3COO)_2 \cdot 4H_2O$ (0.2 mol) were put into a ball mill (ball and powder weight ratio of 15:1) for 5 h. The obtained precursor was pre-treated at 500 °C for 5 h, then sintering at 750 °C for 12 h to prepared $LiMn_2O_4$ (nominated as LMO-S).

The reactions of synthesized LMO-S can be summarized as follows:

$$\mathrm{LiAc+2Mn(Ac)_2}+\frac{51}{4}\mathrm{O_2}\xrightarrow{750^{\circ}\mathrm{C}}\mathrm{LiMn_2O_4}+10\mathrm{CO_2}+\frac{15}{2}\mathrm{H_2O} \qquad (3)$$

2.2. Structural characterization and electrochemical tests

X-ray diffraction (XRD, D8 advance, Bruker) was employed to identify the crystalline phase of $LiMn_2O_4$ samples with Cu Kα radiation. Scanning electron microscopy (SEM, VEGA3-XMU) was used to characterize the morphology of $LiMn_2O_4$ samples.

$LiMn_2O_4$ material (85 wt.%), acetylene black (10 wt.%) and polyvinylidene fluoride (PVDF, 5 wt.%) as binder were mixed in N-methyl pyrrolidone (NMP) to form the slurry. After the electrode slurries were coated on Al foils, heated at 120 °C for 12 h under vacuum. Then the electrodes were cut into 15.6 mm diameter disks.1M $LiPF_6$ was dissolved in ethylene carbonate (EC) and dimethyl carbonate (DMC) (EC: DMC = 1:1vol%) used as the electrolyte; Li foils (Φ = 14 mm, d = 0.5mm) and Celgard 2500 films were applied as anode electrode and separator, respectively.

Galvanostatic charge/discharge cycles of as-synthesized samples were tested employing NEWARE battery test system (NewareCo.，Ltd.，China) in a voltage range of 3.0 to 4.3 V at room

temperature. Cyclic voltammetry (CV, 3.3-4.5 V) test and electrochemical impedance (EIS, 10^{-2}-10^{5} Hz) test were both performed using CHI-660E electrochemical workstation.

3. RESULTS AND DISCUSSION

3.1. XRD analysis

The XRD patterns of LMO-C and LMO-S are illustrated in Fig. 2. Both the samples exhibited practically identical XRD peaks, both samples exhibited peaks at 2θ were 18.65, 36.13, 37.96, 44.25, 48.31, 58.09, 63.78, and 67.29, which were match the reflections of (111), (311), (222), (400), (311), (511), (440) and (531) for spinel $LiMn_2O_4$ planes (JCPDS: 35-0782, space group: *Fd*-3*m* [25,26]), respectively. It manifested that $LiMn_2O_4$ without any impurity could be prepared by both sodium carbonate co-precipitation route and high temperature solid phase methods.

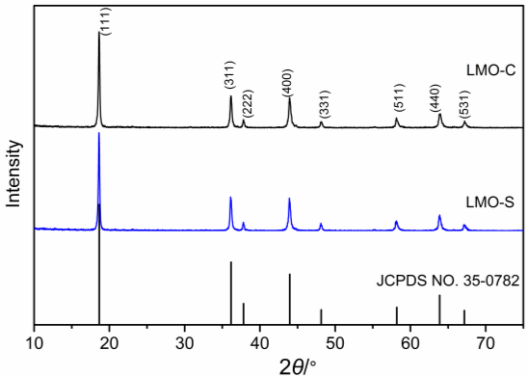

Figure 2. XRD patterns of LMO-C and LMO-S.

3.2. SEM analysis

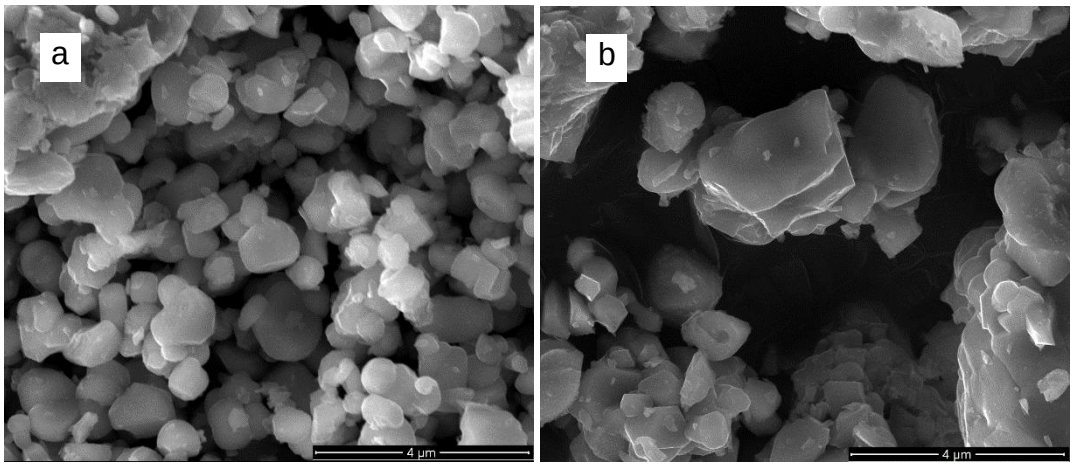

Figure 3. SEM images of (a) LMO-C and (b) LMO-S.

Figure 3 shows the SEM images of the LMO-C and LMO-S. As shown in Fig. 3, the particles of LMO-C were spherical, and the particle size was mainly distributed in 0.50-1.5 μm. LMO-S had particles of agglomerates, with average particle sizes in the range of 0.5-3.0 μm. Compared with LMO-S, the average particle size of LMO-C was small and the distribution was uniform. The small particle could shorten lithium-ion diffusion path and enhance the diffusion of lithium-ion [27,28].

3.3. Electrochemical performances

In order to test the charge-discharge performance of as-synthesized $LiMn_2O_4$ materials, LMO-C and LMO-S were assembled into a button cell for testing. Fig. 4 (a) shows the initial charge and discharge curves of LMO-C and LMO-S at a rate of 0.2 C, respectively. The initial charge and discharge capacity were 123.9 and 114.5 $mAh \cdot g^{-1}$ for LMO-C with a coulombic efficiency of 92.4%, while the first charge and discharge capacity were 122.4 and 105.7 $mAh \cdot g^{-1}$ for LMO-S with a coulombic efficiency of 86.4%. LMO-C exhibited a bigger first discharge capacity and coulombic efficiency than those of LMO-S.

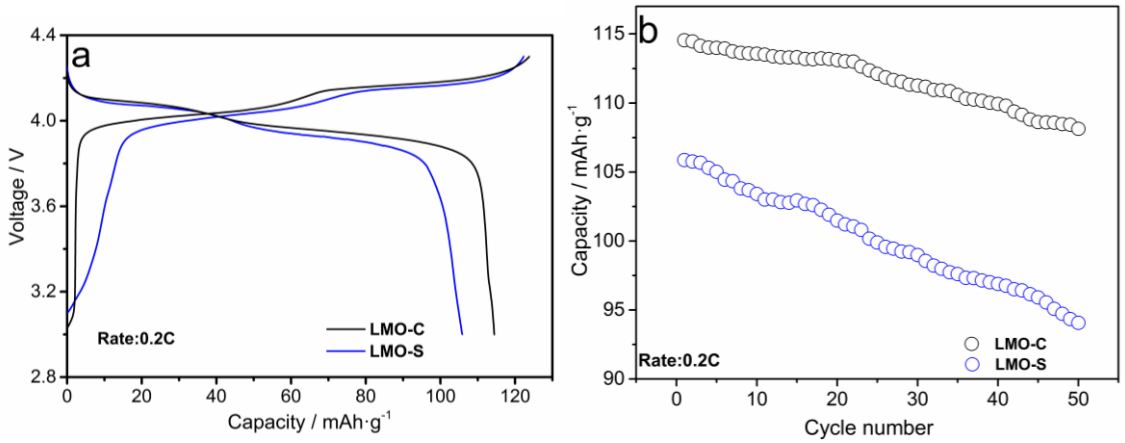

Figure 4. (a) the initial charge/discharge curves and (b) cycling performance of LMO-C and LMO-S at 0.2 C-rate.

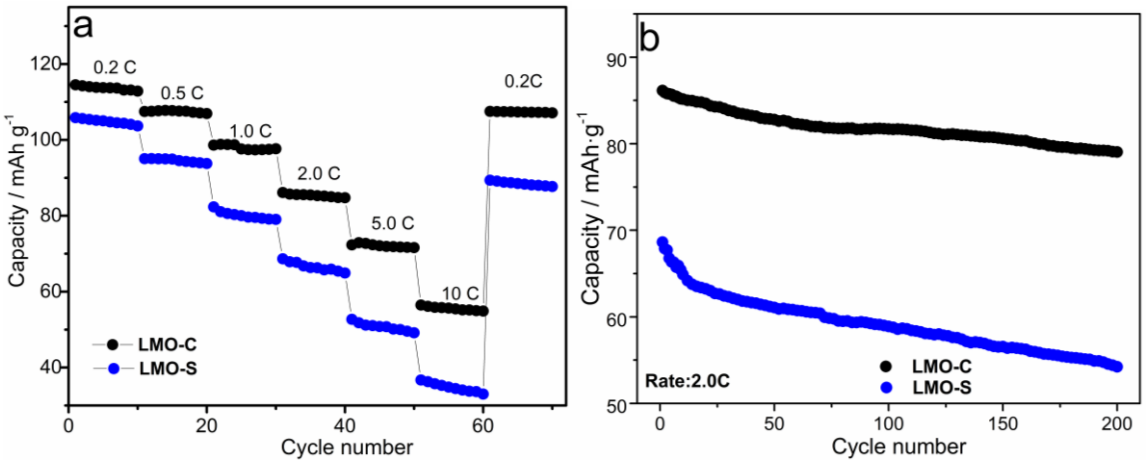

Figure 5. (a) the rate performance and (b) cycling performance of LMO-C and LMO-S at 2.0 C-rate.

Figure 4 (b) shows the cycling performance of LMO-C and LMO-S at 0.2 C-rate, respectively. After 50 cycles, the discharge capacities capacity retentions of LMO-C and LMO-S were 94.2% (107.9 $mAh \cdot g^{-1}$) and 88.5% (93.9 $mAh \cdot g^{-1}$), respectively. It means that LMO-C had a better stability.

Figure 5(a) shows the rate performance of LMO-C and LMO-S at different current rates. The results of both samples were shown in Table 1. LMO-C displayed higher discharge capacities at various current rate than those of LMO-S. Moreover, after 60 cycles, the rate got back to 0.2 C again, the discharge capacity recovery rate for LMO-C was 93.9% (107.5 $mAh \cdot g^{-1}$), while the discharge capacity recovery rate for LMO-S was 84.6% (89.6 $mAh \cdot g^{-1}$). LMO-C showed a better rate capability than LMO-S.

Table 1. Rate performances of LMO-C and LMO-S at various C-rates.

Samples	Rate capability/$mAh \cdot g^{-1}$					
	0.2 C	0.5 C	1.0 C	2.0 C	5.0 C	10 C
LMO-C	114.5	107.3	98.6	82.1	72.3	56.4
LMO-S	105.7	95.0	82.3	68.6	52.5	36.7

In order to further investigate the cycling performance of LMO-C and LMO-S. Fig. 5(b) shows the cycling performance of LMO-C and LMO-S at 2.0 C. It can be see that the cycling curve of LMO-C was always on top of curve for LMO-S. After 200 cycles, the discharge capacity for LMO-C was 79.1 $mAh \cdot g^{-1}$ with a capacity retention of 91.9%, while the discharge capacity for LMO-S was 54.2 $mAh \cdot g^{-1}$ with a capacity retention of 79.0%. LMO-C showed a better cycling performance.

The electrochemical test results illustrated that, LMO-C had a better electrochemical performance than that of LMO-S. The reason for this is that the average particle size LMO-C was smaller, small particle could shorten lithium-ion diffusion path and enhance the diffusion of lithium-ion.

Figure 6 shows cyclic voltammetry (CV) of LMO-C and LMO-S carried out from 3.3 to 4.5 V at 0.1 $mV \cdot s^{-1}$. The CV curves of both samples were similar and had two pairs of anodic/cathodic peaks, corresponding to two-stage reaction processes of lithium-ions intercalation/de-intercalation of $LiMn_2O_4$ crystal [29,30]. The results were consistent with the initial charge/discharge curves in Fig. 4(a).

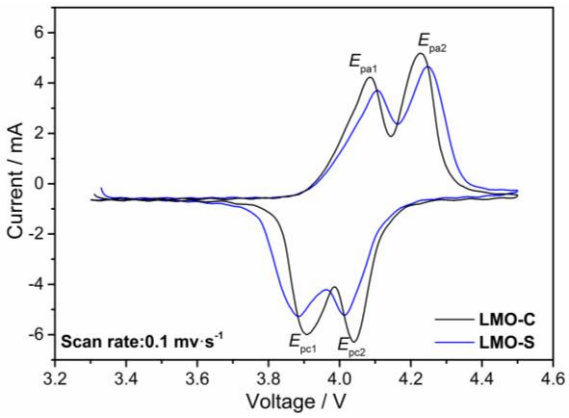

Figure 6. CV curves of LMO-C and LMO-S (0.1 $mV \cdot s^{-1}$).

Table 2. Peak parameters of CV curves of LMO-C and LMO-S; ΔE_p is the separation between E_{pa} and E_{pc}.

Sample	E_{pa1}/V	E_{pa2}/V	E_{pc1}/V	E_{pc2}/V	ΔE_{p1}/mV	ΔE_{p2}/mV
LMO-C	4.095	4.235	3.905	4.031	190	204
LMO-S	4.110	4.251	3.883	4.013	227	238

Table 2 shows the peak parameters of CV curves. LMO-C (190 mV /204 mV) had smaller ΔE_p than LMO-S (227 mV /238 mV). The smaller ΔE_p indicating the faster intercalation and de-intercalation process of lithium-ion [31]. The results were consistent with the galvanostatic testing results.

The EIS curves for LMO-C and LMO-S are illustrated in Fig. 7(a). Both samples exhibited a semicircle in high frequency and an inclined line in low frequency. The equivalent circuit is shown in Fig. 7(a). R_s represents the resistance of electrolyte; R_{ct} represents the charge-transfer of lithium-ion [32,33]; Z_W relates to the Warburg impedance; *CPE* denotes the analog capacitive element.

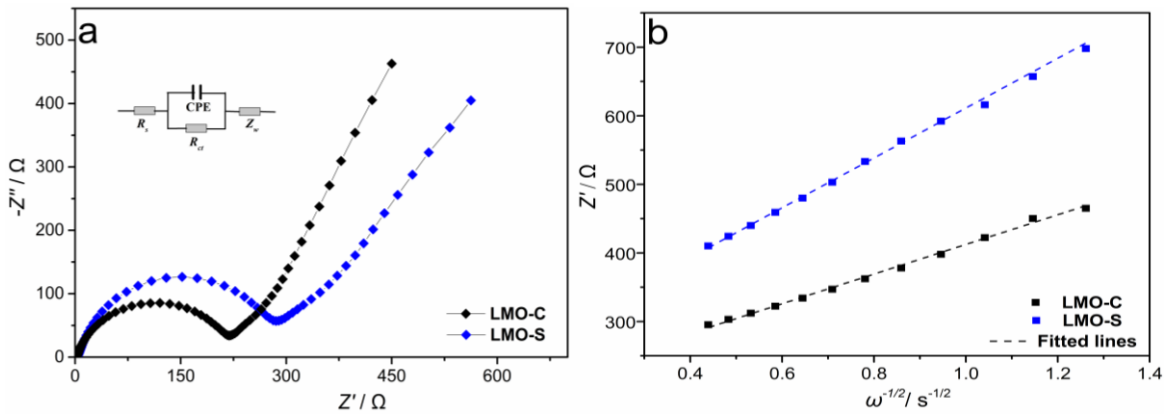

Figure7. (a) EIS curves and relationship between Z' and $\omega^{-1/2}$ for LMO-C and LMO-S before cycle.

The diffusion coefficient of lithium-ion (D_{Li}) can be obtained by the follow equation [8,35]:

$$D_{Li} = R^2T^2/(2A^2n^4F^4C^2\sigma^2) \quad (4)$$

where R is the gas constant (8.314 J·K^{-1}·mol^{-1}); T is the absolute temperature (298 K); n is the electron transfer number (n = 1); A is the surface area of the electrode (1.91 cm^2); F is the Faraday constant (96485 C·mol^{-1}); C is the initial concentration of lithium-ion in $LiMn_2O_4$, which is 0.02378 mol·cm^{-3} here [19,34]. σ is the Warburg factor. σ has a relationship with Z'. R_s, R_{ct} and the angular frequency (ω), as shown in equation (5) [35]:

$$Z' = R_{ct} + R_s + \sigma\omega^{-1/2} \quad (5)$$

σ can be calculated from Fig.7 (b). The results of the EIS are declared in Table 3.

Table 3. Electrochemical impedance spectroscopy values of LMO-C and LMO-S samples.

Sample	R_s/Ω	R_{ct}/Ω	σ	D_{Li}/cm^2·s^{-1}
LMO-C	2.89	217.6	213.8	7.51×10^{-16}
LMO-S	3.10	290.3	352.3	2.76×10^{-16}

As illustrated in Table 3, the initial R_s of both samples were nearly the same. However, the values of R_{ct} for LMO-C was 217.6 Ω, compared with that of LMO-S (290.3 Ω), LMO-C had a smaller R_{ct}. The smaller R_{ct} was beneficial to overcome the kinetic limitations during the intercalation/de-intercalation process of lithium-ion, while it could improve the diffusion of lithium-ion [36].

The diffusion coefficient of lithium-ion (D_{Li}) for LMO-C (7.51×10^{-16} cm^2·s^{-1}) was larger than LMO-S (2.76×10^{-16} cm^2·s^{-1}). The large lithium-ion diffusion coefficient (D_{Li}) was conducive to the large current charge and discharge of the electrode [37]. It is regarded as a reason why LMO-C had a better electrochemical property than that of LMO-S. The results corresponded to the results of the rate performance curves in Fig. 5(a).

Table 4 shows the related electrochemical data of $LiMn_2O_4$ cathode material prepared by different synthesis methods which have been reported. It this work, $LiMn_2O_4$ cathode material has been prepared by sodium carbonate co-precipitation route, sodium carbonate co-precipitation route can simultaneously make Li^+ and Mn^{2+} precipitate, thereby obtaining a more uniform $Li_2CO_3·2MnCO_3$ as precursor, and can reduce the reaction steps and improve the efficiency. Moreover, the obtain $LiMn_2O_4$ showed an excellent electrochemical performance.

Table 4. Performance parameters of $LiMn_2O_4$ synthesized by different synthesis methods.

Synthesis method	Rate capacity (mAhg^{-1})	References
Sodium carbonate co-precipitation	114.5 (0.2 C); 107.3 (0.5 C); 98.6 (1.0C)	As prepared
Solid state reaction	108.6 (0.1 C); 105.3 (0.2 C); 92.5 (1.0C)	[18]
High temperature ball milling	109.5 (0.5C); 98.3 (1.0C); 86.5 (2.0C)	[21]
Sol-gel method	114 (0.5 C) 82 (1.0 C)	[24]

4. CONCLUSIONS

In this work, $LiMn_2O_4$ cathode materials were synthesized via sodium carbonate co-precipitation route and high temperature solid phase methods. The effect of different synthetic methods on the electrochemical performances of $LiMn_2O_4$ were investigated by XRD, SEM, galvanostatic testing, CV and EIS. XRD analysis revealed that both LMO-C and LMO-S showed a single phase without any impurity; SEM analysis revealed LMO-C had a smaller average particle size than that of LMO-S; Galvanostatic testing, CV and EIS results indicated LMO-C had better electrochemical performances than LMO-S. Thus, this study paves a facile and eco-friendly sodium carbonate co-precipitation approach to synthesis $LiMn_2O_4$ cathode material.

ACKNOWLEDGMENTS
This research did not receive any specific grant from funding agencies in the public, commercial, or not-for-profit sectors.

References

1. A.K. Padhi, K.S. Nanjundaswamy and J.B. Goodenough, *J. Electrochem. Soc.,* 144 (1997) 1188.
2. Z. Li, J. Zhang, J. Shu, J. Chen, C. Gong, J. Guo, L. Yu and J. Zhang, *J. Power Sources*, 381 (2018)
3. A. Eddahech, O. Briat and J. Vinassa, *Electrochim. Acta,* 114 (2013) 750.
4. F. Lin, D. Nordlund, Y. Li, M.K. Quan, L. Cheng, T.C. Weng, Y. Liu, H.L. Xin and M.M. Doeff, *Nat. Energy*, 1 (2016) 15004.
5. I. Bezza, E. Luais, F. Ghamouss, M. Zaghrioui, F. Tran-van and J. Sakai, *J. Alloys Compd.,* 805 (2019) 19.
6. Y. Cho, M. HwanLee, H. Kim, K. Ku, G. Yoon, S.K. Jung, B. Lee, J. Kim and K. Kang, *Mater. Res. Bull.,* 96 (2017) 524.
7. W. Tang, L.L. Liu, S. Tian, L. Li, L.L. Li, Y.B. Yue, Y. Bai, Y.P. Wu, K. Zhu and R. Holze, *Electrochem. Commun.,* 13 (2011) 1159.
8. Y. Chen, Y. Tian, Y. Qiu, Z. Liu, H. He, B. Li and H. Cao, *Materials Today Advances*, 1 (2019)1.
9. R.A. Rodríguez, E.L. Pérez-Cappe, Y.M. Laffita, A.C. Ardanza, J.S. Salazar, M.Á. Santos, M.A. Aguilar Frutis, N.D.S. Mohalem and O.L. Alves, *Solid State Ionics,* 324 (2018) 77.
10. C. Zhang, X. Liu, Q. Su, J. Wu, T. Huang and A. Yu, *ACS Sustain. Chem. Eng.,* 5 (2017) 640.
11. S. Yang, D.O. Schmidt, A. Khetan, F. Schrader, S. Jakobi, M. Homberger, M. Noyong, A. Paulus, H. Kungl and R.A. Eichel, *Materials*, 11 (2018) 806.
12. Y. Hou, K. Chang, H. Tang, B. Li, Y. Hou and Z. Chang, *Electrochim. Acta*, 319 (2019) 587.
13. K. Park, J.H. Park, S.G. Hong, J. Yoon, S. Park, J.H. Kim, D. Yoon, H. Kim, Y.H. Son, J.H. Park and S. Kwon, *Electrochim. Acta,* 222 (2016) 830.
14. A. Li, Z. Shao, S. Yang, X. Li and A. Zhang, *Ionics,* (2020) https://doi.org/10.1007/s11581-019-03432-4.
15. K. Hariprasad, N. Naresh, B. Nageswar Rao, M. Venkateswarlu and N. Satyanarayana, *Materials Today: Proceedings*, 3 (2016) 4040.
16. Z. Zou, Z. Li, H. Zhang, X. Wang and C. Jiang, *J. Mater. Sci. Technol.*, 33 (2017) 781.
17. T. Kozawa, K. Yanagisawa, T. Murakami and M. Naito, *J. Solid State Chem.,* 243 (2016) 241.
18. B.S. Liu, Z.B. Wang, Y. Zhang, F.D. Yu, Y. Xue, K. Ke and F.F. Li, *J. Alloys Compd.*, 622 (2015) 902.
19. X. Li, L. Yu, Y. Zhang, H. Shao and W. Zhang, *Ionics*, 26 (2020) 1591.

20. X.W. Lv, S.L. Chen, C. Chen, L.H. Liu, F. Liu and G.H. Qiu, *Solid State Sci.,* 31 (2014) 16.
21. Q. Zhao, X. Li, Z. Shao, B. Xu, C. Liu and M. Jiang, *Int. J. Electrochem. Sci.,* 13 (2018) 3691.
22. R. Thirunakaran, G.H. Lew and W.S. Yoon, *J. Electroanal. Chem.,* 767 (2016) 141.
23. Z. Yang, Y. Jiang, H.H. Xu and Y.H. Huang, *Electrochim. Acta,* 106 (2013) 63.
24. C.Y. Wan, M.C. Wu and D. Wu, *Powder Technol.,* 199: (2010) 154.
25. J. Liu, J. Hao, J. Guo, C. Su and R. Wang, *Int. J. Electrochem. Sci.,* 11 (2016) 5838.
26. L. Tian, C. Su, Y. Wang, B. Wen, W. Bai and J. Guo, *Vacuum,* 164 (2019) 153.
27. X. Li, L. Yu, H. Shao and W. Zhang, *Int. J. Mod. Phys. B,* 34 (2020) 2050047.
28. X. Li, Y. Cui, L. Yu, H. Shao, Z. Shao, C. Li and Z. Shao, *Ionics*, 25 (2019) 4597.
29. Y. Cai, Y. Huang, X. Wang, D. Jia, W. Pang, Z. Guo and X. Tang, *J. Power Sources*, 278 (2015) 574.
30. H.Y. Zhao, F. Li, X.Q. Liu, W.Q. Xiong, B. Chen, H.L. Shao, D.Y. Que, Z. Zhang and Y. Wu, *Electrochim. Acta,* 166 (2015) 124.
31. X. Li, L. Yu, Y. Cui, A. Li, H. Shao, Z. Shao, W. Zhang and Z. Shao, *Int. J. Hydrogen Energy,* 44 (2019) 27204.
32. H.Q. Wang, F.Y. Lai, Y. Li, X.H. Zhang, Y.G. Huang, S.J. Hu and Q.Y. Li, *Electrochim. Acta,* 177 (2015) 290.
33. Y. Lee, T.Y. Kim, D.W. Kim, J.K. Lee and W. Choi, *J. Electroanal. Chem.,* 736 (2015) 16.
34. D.L. Guo, X.G. Wei, Z.R. Chang, H.W. Tang, B. Li, E. Shangguan, K. Chang, X.Z. Yuan and H.J. Wang, *J. Alloys Compd.,* 632 (2015) 222.
35. P.R. Ilango, K. Prasanna, S.J. Do, Y.N. Jo and C.W. Lee, *Sci. Rep.,* 6 (2016) 29826.
36. B. Han, X.D. Meng, L. Ma and J.Y. Nan, *Ceram. Int.,* 42 (2016) 2789.
37. F. Yao, F. Günes, H.Q. Ta, S.M. Lee, S.J. Chae, K.Y. Sheem and Y.H. Lee, *J. Am. Chem. Soc.,* 134 (2012) 8646.